Current-Sourcing Push-Pull Parallel-Resonance Inverter (CS-PPRI): Theory and Application as a Discharge Lamp Driver

Michael Gulko and Sam Ben-Yaakov, *Member, IEEE*

Abstract— **A novel topology, current-sourcing push-pull parallel-resonance inverter (CS-PPRI) was investigated theoretically and experimentally. The proposed power stage is built around a current fed push-pull inverter. The main features of the proposed inverter are: a load independent output current and zero voltage switching (ZVS). It is suggested that the proposed CS-PPRI is a viable alternative for realizing electronic ballasts for low and high-intensity discharge lamps.**

I. Introduction

LOW- and high-intensity discharge lamps [1] are universally recognized as the most efficient method of illumination. They require however, an extra circuitry to regulate the current thru the lamps. Electronic ballasts [1], [2] are useful not only to enable operation from a battery source, but also to facilitate dimming, to reduce the overall size of the "ballast" and to eliminate line frequency flickering [1], [3], [4]. An extra bonus of a high frequency of operation is the increase in illumination per a given electrical input power [3], [4], [5].

Discharge lamps are an example of a family of loads that call for a current source rather than a voltage source drive. The direct approach for handling these design problems is therefore to develop a current sourcing inverter rather than using a voltage source in series with a ballast. The objective of this study was to examine this approach by investigating a novel modification of the current fed inverter topology [6].

II. Topology

The proposed topology (Fig. 1) is similar to the push-pull parallel-resonance configuration described previously [7]. The basic components of this stage are an input inductor (L_{in}), a parallel resonance circuit (C_r, L_r) and symmetrically driven switches (Q_1, Q_2). However, unlike the classical loading method, the proposed current-sourcing push-pull parallel-resonance inverter (CS-PPRI) is serially loaded. Serial coupling for a full bridge current fed inverter topology was previously described [6]. Here we present a series coupling method which is suitable for push-pull stages. In the proposed CS-PPRI (Fig. 1), load coupling is carried out via a current transformer which includes a split primary. The purpose of this configuration is to retain the symmetrical operation of the push-pull stage by balancing the resistive load seen by each half of the circuit.

Manuscript received March 3, 1993; revised September 19, 1993.

The authors are with the Department of Electrical and Computer Engineering, Ben-Gurion University of the Negev, Beer-Sheva 84105, Israel.

IEEE Log Number 9200213.

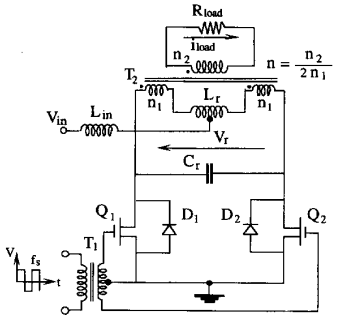

Fig. 1. The proposed current-sourcing push-pull parallel-resonance inverter (CS-PPRI).

The basic operation of the proposed inverter is described by considering the equivalent circuit of the CS-PPRI (Fig. 2(a)) in which the load is reflected to the primary and the input inductor (L_{in}) is replaced by a dc current source. The latter is justified by the fact that in the proposed design [7]

$$4L_{\text{in}} \gg L_r \tag{1}$$

where L_r is the resonant inductor. Hence, the ac current component thru L_{in} will be low and therefore the input current during a resonance cycle can be considered constant.

As previously described [7], the operation of this stage when driven by a switching frequency (f_s) which is a lower than the resonance frequency (f_r), is characterized by two distinct modes: the quasiresonance mode and the boost mode (Fig. 2(b), (c)). For each half switching frequency cycle (f_s), the voltage waveform across the tank (V_r) will therefore be a quasisinusoidal shaped signal of (T_λ) duration and zero volt during the boost period T_{boost} (Fig. 3).

In response to the voltage across the parallel resonance network, the resonant inductor current (i_L) and hence the current thru the load, will be continuous and smooth (Fig. 3). Since the transitions from one mode to the other is carried out when the voltage across the tank is nil, the transistors (Q_1, Q_2) operate under zero voltage switching (ZVS). This helps to reduce switching losses at high-operating frequency. The experimental CS-PPRI was tested at a switching frequency range of 250 to 450 kHz.

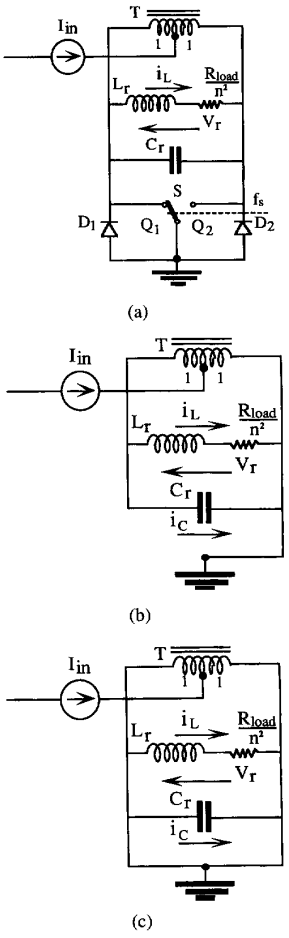

Fig. 2. Simplified equivalent circuit of the proposed CS-PPRI (a) and general representation for the resonance mode (b) and the boost mode (c).

III. ANALYSIS

A. Assumptions

Analytical expressions of the basic parameters of the CS-PPRI were developed under the assumptions that the switches, diodes and transformers are ideal, the input inductance of L_{in} is much larger than the tank inductance of L_r and that the parasitic inductances and capacitances are negligible small.

B. Basic Voltage and Current Waveforms

The expression for the tank voltage (v_r) at the quasiresonant period (Fig. 3(a)) and (T_λ, Fig. 3) can be derived by solving the following set of differential equations

$$\frac{I_{\text{in}}}{2} = i_C + i_L \tag{2}$$

$$v_r = \frac{1}{C_r}\int i_C dt \tag{3}$$

$$v_r = L_r\frac{di_L}{dt} + i_L\frac{R_{\text{load}}}{n^2} \tag{4}$$

The general solution of the set of differential equations (2–4) has the form

$$v_r = e^{-\frac{R_{\text{load}}}{2n^2L_r}t}[A_1\sin(\omega_r t) + A_2\cos(\omega_r t)] + \frac{R_{\text{load}}}{n^2}\frac{I_{\text{in}}}{2} \tag{5}$$

where

R_{load}	Load resistor (Fig. 1)
n	Turns ratio of transformer T_2 (Fig. 1)
I_{in}	Input current (Fig. 2(a))

$$\omega_o = \frac{1}{\sqrt{L_rC_r}}$$

$$\omega_r = \omega_o\sqrt{1-\left(\frac{1}{2Q}\right)^2}$$

$$Q = \frac{n^2}{R_{\text{load}}}\sqrt{\frac{L_r}{C_r}}.$$

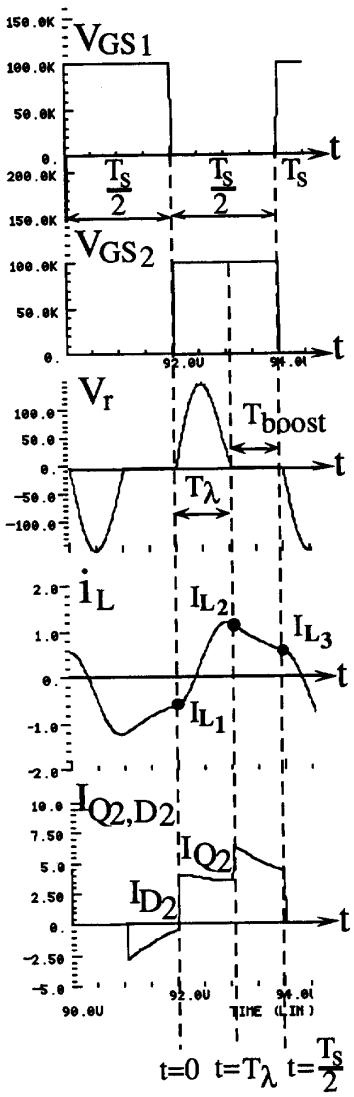

Fig. 3. Expected waveforms of proposed CS-PPRI. (Simulated by HSPICE, Meta Software Co.).

The integration constants A_1 and A_2 are found by the boundary conditions constrains which require that $v_r = 0$ at $t = 0$ and when $t = T_\lambda$ (Fig. 3). Applying these relationships, the tank voltage (v_r) is found to be

$$v_r = \frac{R_{\text{load}} I_{\text{in}}}{2n^2}\left[\left(\frac{\cos(\vartheta_\lambda) - e^{\alpha}}{\sin(\vartheta_\lambda)}\right)e^{-\alpha x}\sin(\vartheta_\lambda x) - e^{-\alpha x}\cos(\vartheta_\lambda x) + 1\right] \tag{6}$$

where

$$\alpha = \frac{\vartheta_\lambda R^*}{\sqrt{4 - R^{*2}}}$$
$$\vartheta_\lambda = \omega_r T_\lambda$$
$$R^* = \frac{1}{Q} - \text{Normalized load resistance}$$
$$x = \frac{t}{T_\lambda}.$$

At steady-state conditions, the average voltage (per cycle) across L_{in} is zero

$$V_{\text{in}} - \frac{2}{T_s}\int_0^{\frac{T_s}{2}} \frac{v_r}{2} dt = 0. \tag{7}$$

Applying the fact that during the T_{boost} period $\{T_\lambda < t < \frac{T_s}{2}\}$ (Fig. 3) $v_r = 0$

$$V_{\text{in}} = \frac{\alpha}{\pi R^*}\frac{f_s}{f_o}\int_0^1 v_r dx \tag{8}$$

where

$$f_o = \frac{\omega_o}{2\pi}.$$

Integrating (8), assuming that the CS-PPRI is lossless and equating input to output power, we obtain

$$I^*_{\text{load}} = \frac{2}{R^*}\left[\frac{\frac{2\pi\alpha\sin(\vartheta_\lambda)}{\vartheta_\lambda R^*}}{\left(\frac{4\alpha^2}{\vartheta_\lambda R^{*2}}\right)\sin(\vartheta_\lambda) + 2\cos(\vartheta_\lambda) - (e^{\alpha} + e^{-\alpha})}\frac{f_o}{f_s}\right]^{\frac{1}{2}} \tag{9}$$

where
$I^*_{\text{load}} = I_{\text{load}_{(\text{rms})}}\frac{n}{V_{\text{in}}}\sqrt{\frac{L_r}{C_r}}$ – Normalized load current.

The relationship between the quasiresonant period (T_λ), the major parameter of the inverter and the frequency ratio (f_o/f_s) is derived by applying the fact that during the boost period (T_{boost}, (Fig. 3)), inductor L_r and resistor $\frac{R_{\text{load}}}{n^2}$ are shorted (Fig. 3(b)) and hence the inductor current i_L through this network is decaying exponentially

$$\frac{I_{L2}}{I_{L3}} = e^{-\frac{T_{\text{boost}}}{\tau}} \tag{10}$$

where I_{L2} and I_{L3} are the boundary inductor currents (Fig. 3) and $\tau = \frac{L_r n^2}{R_{\text{load}}}$-the time constant of $\frac{R_{\text{load}}}{n^2}L_r$ circuit (Fig. 3(b)). Utilizing the fact that the resonant inductor current (i_L) is

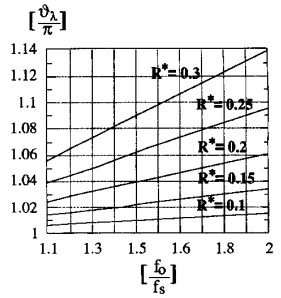

Fig. 4. The normalized quasiresonant period ($\frac{\vartheta_\lambda}{\pi} = 2f_r T_\lambda$) as a function of the normalized switching frequency $\left(\frac{f_o}{f_s}\right)$with the normalized load (R^*) as a parameter.

symmetrical $I_{L3} = -I_{L1}$ (Fig. 3), from (2) and (3), we find (11)

$$i_L = \frac{I_{\text{in}}}{2}\left[1 - \frac{\vartheta_\lambda R^{*^2}}{2\alpha}e^{-\alpha x}\left(\left(\frac{\cos(\vartheta_\lambda) - e^{\alpha}}{\sin(\vartheta_\lambda)}\right) \times \left(\cos(\vartheta_\lambda x) - \frac{\alpha\sin(\vartheta_\lambda x)}{\vartheta_\lambda}\right) + \frac{\alpha\cos(\vartheta_\lambda x)}{\vartheta_\lambda} + \sin(\vartheta_\lambda x)\right)\right]. \tag{11}$$

Applying now (11), the fact that the boundary conditions are: $i_L = I_{L1}$ at $t = 0$ ($x = 0$) and $i_L = I_{L2}$ when $t = T_\lambda (x = 1)$ (Fig. 3) and the exponential behavior of the inductor current (i_L) (10), the frequency ratio (f_o/f_s) is expressed as

$$\frac{f_o}{f_s} = \frac{2}{\pi R^*}\left[\frac{1}{2}\ln \times\left(-\frac{(2 - R^{*2})\sin(\vartheta_\lambda) + \frac{\vartheta_\lambda R^{*2}}{\alpha}(\cos(\vartheta_\lambda) - e^{-\alpha})}{(2 - R^{*2})\sin(\vartheta_\lambda) - \frac{\vartheta_\lambda R^{*2}}{\alpha}(\cos(\vartheta_\lambda) - e^{\alpha})}\right) - \alpha\right]. \tag{12}$$

The last equation can be used to explore the dependence of the quasiresonant angle ($\vartheta_\lambda = \omega_r T_\lambda$) on the switching frequency (f_s) and load (R_{load}) (Fig. 4). It is evident that under the operating conditions discussed here, the quasiresonant period is longer than half the period of the natural resonant frequency (f_o).

C. Voltage Stresses

Assuming that the voltage waveform v_r (Fig. 3) could be approximated by a sinusoidal waveform [7], and applying (8), we find the maximum tank voltage (V_{rm}) which is the voltage stress of the transistors (V_{Qm}) and the diodes (V_{Dm})

$$V_{Qm} = V_{Dm} = V_{rm} = \frac{V_{\text{in}}\pi^2 R^*}{2\alpha}\frac{f_o}{f_s}. \tag{13}$$

D. Current Stresses

The maximum normalized transistor current I^*_{Qm} (Fig. 5(a)) was found to be

$$I^*_{Qm} = I_{Qm}\frac{\omega_o L_r}{V_{\text{in}}} = I^{*2}_{\text{load}} R^*\left(\frac{1}{2} + \frac{1}{4\sin(\vartheta_\lambda)}\right.$$

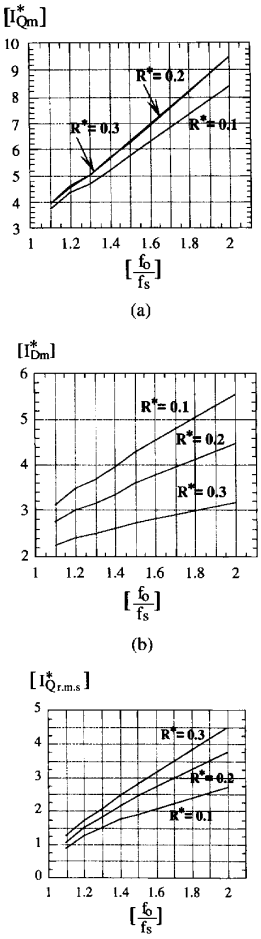

Fig. 5. Transistors and diodes current stresses as a function of the normalized switching frequency $\left(\frac{f_o}{f_s}\right)$ with the normalized load (R^*) as a parameter. (a) Normalized transistor current (I^*_{Qm}). (b) Normalized diode current (I^*_{Dm}). (c) Normalized rms transistor current ($I^*_{Q\text{rms}}$).

$$\times \left[(2 - R^{*2})\sin(\vartheta_\lambda) + \frac{\vartheta_\lambda R^{*2}}{\alpha}\left(\cos(\vartheta_\lambda) - e^{-\alpha}\right)\right]\Bigg). \tag{14}$$

The maximum normalized diode current (I^*_{Dm}) (Fig. 5(b)) was derived to be

$$I^*_{Dm} = I_{Dm}\frac{\omega_o L_r}{V_{\text{in}}} = I^*_{Qm} - I^{*2}_{\text{load}}R^*. \tag{15}$$

The transistors' normalized rms current $I^*_{Q\text{rms}}$ was evaluated and is shown in Fig. 5(c) in a normalized form $\left(I^*_{Q\text{rms}}\right)$

$$I^*_{Q\text{rms}} = I_{Q\text{rms}}\frac{\omega_o L_r}{V_{\text{in}}}. \tag{16}$$

IV. Experimental Results

The design parameters of the experimental CS-PPRI were as follows: $V_{\text{in}} = 24$ V; $L_{\text{in}} = 70$ μH; $C_r = 8.24$ nF; $n = 4$; $f_o = 487.9$ kHz; $L_r = 12.9$ μH (including 1.6 μH of leakage inductor of the transformer T_2).

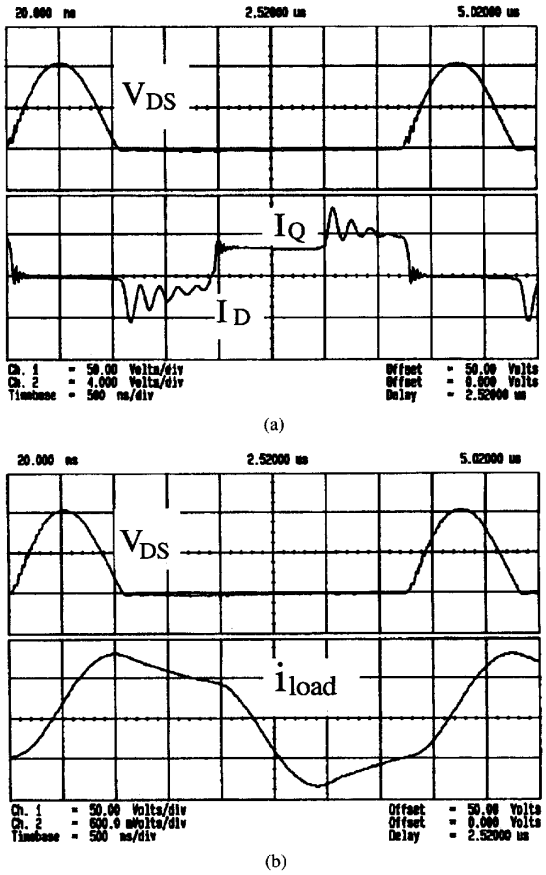

Fig. 6. Measured waveforms of experimental CS-PPRI. Vertical scales (a) 50 V/div, 2 A/div and (b) 0.6 A/div. Horizontal scales: 500 nS/div.

The waveforms of the experimental circuit (Fig. 6) were found to be smooth and indicative of ZVS (Fig. 3). The parasitic oscillation of the current thru the switch is partially due to a layout modification required to facilitate current measurements (an extra loop at the drain of one of the transistors). It should be pointed out though, that a slight parasitic oscillation does not interfere with the inherent ZVS of the proposed CS-PPRI. The smooth operation of the CS-PPRI dispose of the need to use snubbers or clamps.

The output current for various load resistances (Fig. 7) were found to be in good agreement with the analytical expected values (9). The somewhat larger discrepancy at high-frequency ratios (f_o/f_s) is due to conductive losses which increase as the boost period is becoming longer. Since parasitic losses were ignored in the present theoretical analysis, one would expect an inconsistency between the analytical and experimental results when the losses are high.

The theoretical and experimental results clearly point out to the fact that the proposed CS-PPRI is operating as a current source (Fig. 7) and that the magnitude of the output current is controlled by the driving switching frequency (f_s) (Fig. 8).

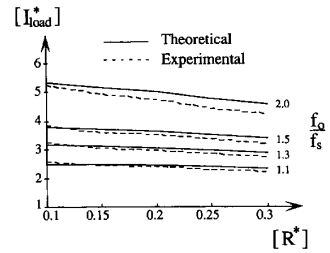

Fig. 7. The relationship between the normalized output current I^*_{load} (9) and the normalized load resistance R^* (12) as a function of the frequency ratio $\left(\frac{f_o}{f_s}\right)$.

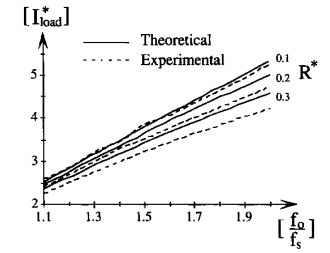

Fig. 8. The relationship between the normalized output current I^*_{load} (9) and the frequency ratio $\left(\frac{f_o}{f_s}\right)$ as a function of the normalized load resistance R^* (12).

The overall efficiency of the experimental CS-PPRI was found to be around 85% for a power level of 80 Watt.

V. Application as a Discharge Lamp Driver

A. Fluorescent Lamp

The current sourcing nature of the proposed CS-PPRI makes it a viable alternative for fluorescent lamp driver. The proposed modification for a battery operated fluorescent lamp driver is shown in Fig. 9. The main difference of this driver as compared to the one shown in Fig. 1, is the inclusion of an extra capacitor (C_{ig}) at the output side. The purpose of this capacitor is to provide initial filament heating path and high voltage during the lamp starting period [1]. This conduction path facilitates a current flow through the filaments (I_h), lowering thereby the voltage required for igniting the lamp. Cold ignitions, i.e., without pre-heating the cathodes is highly undesirable since it shortens the fluorescent lamp life [1]. The capacitor (C_{ig}) and the reflected resonant inductor (L_r) form a series-resonant circuit which generates high voltage (V_{ig}) necessary for lamp ignition [1]. After ignition, the series-resonant circuit ($n^2 L_r C_{\text{ig}}$) is heavily damped by the low impedance of the operating fluorescent lamp. This reduces the capacitor's current and prevents the cathodes from overheating when the fluorescent lamp is in operating. However, if dimming is desired, a residual heaters' current is necessary to prevent lamp quenching [4]. The value of the auxiliary capacitor (C_{ig}, Fig. 9) can be calculated by solving the set

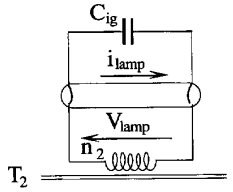

Fig. 9. Output section of the CS-PPRI (Fig. 1) when used as a battery-operated fluorescent lamp driver.

of non-linear equations for no load condition [8]

$$\left[\left(\frac{\omega_{s_{\text{ig}}}}{\omega_{\text{ser}}}\right)^2 - 1\right]\frac{C_r}{n^2 C_{\text{ig}}} = \frac{4\cos\frac{\lambda}{2}\left(1-\cos\frac{\lambda}{2}\right)}{\lambda\left[\left(\frac{\pi}{\lambda}\right)^2 - 1\right]} \tag{17a}$$

$$V_{\text{ig}} = \frac{4nV_{\text{in}}\cos\frac{\lambda}{2}}{\left(1-\frac{\lambda}{\pi}\right)^2\left[\left(\frac{\omega_{s_{\text{ig}}}}{\omega_{\text{ser}}}\right)^2 - 1\right]} \tag{17b}$$

$$I_{h_{(\text{rms})}} = \omega_{s_{\text{ig}}} V_{\text{ig}} C_{\text{ig}} \tag{17c}$$

where,

V_{ig} lamp ignition voltage,
$f_{s_{\text{ig}}}$ ignition switching frequency,
$I_{h_{\text{rms}}}$ filament heating current during ignition,
$\omega_{s_{\text{ig}}} = 2\pi f_{s_{\text{ig}}}$
$\lambda = \omega_{s_{\text{ig}}} T_\lambda$
$\omega_{\text{ser}} = \frac{1}{n\sqrt{L_r C_{\text{ig}}}}$.

As previously documented [1], [3], fluorescent lamps exhibit a resistive nature at high frequencies. This can be clearly seen by examining the experimental lamp voltage and current depicted in Fig. 10(a). It is thus evident that a first order approximation of a fluorescent lamp, when driven by a high-frequency source, is a pure resistor.

B. Design Guidelines

The following procedure is suggested for the practical design of a battery operated CS-PPRI based driver for fluorescent lamps. It is assumed that the following parameters are given: input voltage to the driver (V_{in}), lamp current ($I_{\text{lamp}_{(\text{rms})}}$), lamp power ($P_{\text{lamp}}$), and the recommended ignition peak voltage ($V_{\text{ig}_{\text{pk}}}$) for a given heating current($I_{h_{(\text{rms})}}$):

1) Select the switching frequency (f_s) according to the transistors and magnetic material available.
2) Select I^*_{load} and calculate (n) (17a, b, c)

$$n = \frac{1}{\frac{\pi V_{\text{in}}}{V_{\text{ig}_{\text{pk}}}}\left[\left(\frac{\sqrt{2}I_{h_{(\text{rms})}} I^*_{\text{load}}}{\pi I_{\text{lamp}_{(\text{rms})}}}\right)^2 - 1\right]}.$$

Observe that the normalized output current (I^*_{load}) must be confined to the range

$$I^*_{\text{load}} > \frac{\pi I_{\text{lamp}_{(\text{rms})}}}{\sqrt{2}I_{h_{(\text{rms})}}}$$

to ensure a positive (n). The larger the normalized output current (I^*_{load}) the smaller the (n). It is recommended to

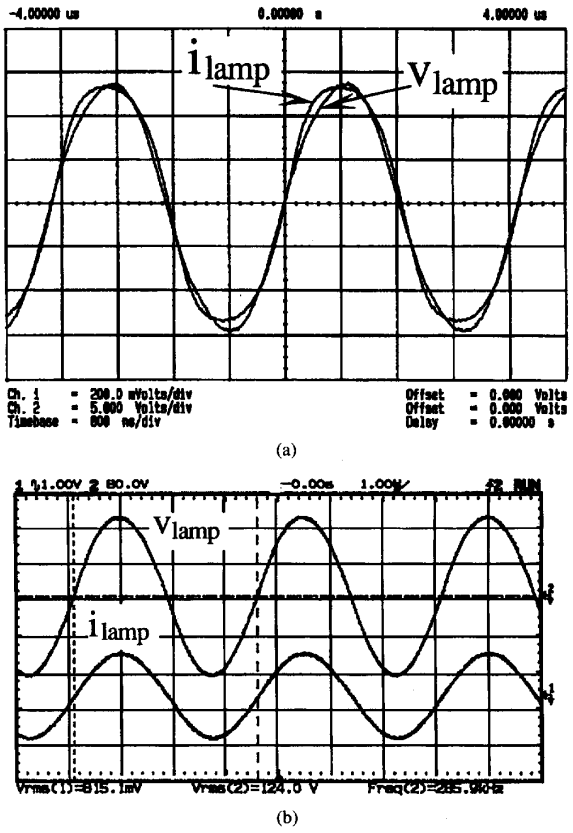

Fig. 10. Experimental waveforms of discharge lamps when driven by proposed CS-PPRI. (a) Fluorescent lamp (General Electric type F40D/2-40 W). Vertical scales: 50 V/div and 0.2 A/div. Horizontal scale: 800 nS/div. (b) Metal halide discharge lamp (Sylvania type H38AV-100/DX-100 W). Vertical scales: 80 V/div and 1 A/div. Horizontal scale: 1 μs/div.

limit (I^*_{load}) to no more than 5, since a large (I^*_{load}) will increase the boost period $\left(\frac{f_o}{f_s}\right)$ (Fig. 8) and will therefore increase switching losses (Fig. 5a, b, c).

3) Calculate the apparent lamp resistance (R_{lamp})

$$R_{\text{lamp}} = \frac{P_{\text{lamp}}}{\eta I^2_{\text{lamp}_{(\text{rms})}}}$$

where ηth efficiency of the CS-PPRI (0.8–0.85).

4) Calculate (R^*)

$$R^* = \frac{R_{\text{lamp}} I_{\text{lamp}_{(\text{rms})}}}{V_{\text{in}} n I^*_{\text{load}}}.$$

The current sourcing nature of the CS-PPRI is effective when the normalized load (R^*) is less than 0.3 (Fig. 7). If the calculated R^* is larger than 0.3, the design steps need to be iterated by reducing I^*_{load} (step 2) and repeating steps (2 and 4).

5) Select the ratio $\left(\frac{f_o}{f_s}\right)$ from Fig. 8 for the chosen I^*_{load} and the calculated R^*.

6) Calculate the natural resonant frequency (f_o) from the ratio $\left(\frac{f_o}{f_s}\right)$.

7) Calculate (L_r) (9)

$$L_r = \frac{I^*_{\text{load}} V_{\text{in}}}{2\pi f_o n I_{\text{lamp}_{(\text{rms})}}}.$$

8) Calculate (C_r) (5)

$$C_r = \frac{1}{L_r (2\pi f_o)^2}.$$

9) Calculate the auxiliary capacitor (C_{ig}) (17)

$$C_{\text{ig}} = \frac{\pi V_{\text{in}} C_r}{n V_{\text{ig}_{\text{pk}}}}.$$

10) Calculate the ignitiion switching frequency $(f_{s_{ig}})$ (17)

$$f_{s_{\text{ig}}} = \frac{\sqrt{2} I_{h_{(\text{rms})}}}{2\pi C_{\text{ig}} V_{\text{ig}_{\text{pk}}}}.$$

11) Estimate the current stress of the transistors (I_{Q_m}) and antiparallel diodes (I_{D_m}) from (14), (15) and Figs. 5a and 5b.

12) Calculate the voltage stress of the transistors (V_{Q_m}) and antiparallel diode (V_{D_m}) from (13).

13) The structural design of (L_r) is based on the required inductance (L_r), maximum voltage (V_{r_m}), rms current $(I_{Lr_{(\text{rms})}}$ and switching frequency (f_s) (9), (13)

$$I_{Lr_{(\text{rms})}} = \sqrt{\left(I_{\text{lamp}_{(\text{rms})^n}}\right)^2 + \left(0.5\frac{V_{\text{in}}(I^*_{\text{load}})^2 R^*}{2\pi f_o L_r}\right)^2}.$$

These constraints normally call for an air gapped construction for L_r.

14) Similarly, transformer (T_2) design is based on the maximum transformer voltage $(V_{Tr_{\max}})$ and current $(I_{Tr_{(\text{rms})}})$ (9), (13), (14)

$$V_{Tr_{\max}} = \frac{V_{\text{in}}}{2\pi f_o L_r}\left(I^*_{Q_m} - 0.5(I^*_{\text{load}})^2 R^*\right)\frac{R_{\text{lamp}}}{n^2}$$

$$I_{Tr_{(\text{rms})}} = I_{Lr_{(\text{rms})}}.$$

15) Choose (L_{in}) such that $4L_{\text{in}} \gg L_r$. Calculate the maximum inductor voltage $(V_{\text{Lin}_{\max}})$ and the inductor current $(I_{\text{Lin}_{(\text{rms})}})$

$$V_{\text{Lin}_{\max}} = \frac{V_{r_m}}{2} - V_{\text{in}}$$

$$I_{\text{Lin}_{(\text{rms})}} = I_{\text{in(dc)}} = \frac{V_{\text{in}}(I^*_{\text{load}})^2 R^*}{2\pi f_o L_r}.$$

These constraints normally call for an air-gapped construction for L_{in}.

16) The resonant capacitor (C_r) must be capable of sustaining the expected maximum voltage $(V_{C_{r_{\max}}} = V_{r_m})$ and should have a low ESR. Silver mica capacitors are recommended.

17) The auxiliary capacitor (C_{ig}) must be capable of sustaining the expected maximum voltage $(V_{C_{\text{ig}}} = V_{\text{ig}_{\text{pk}}})$

C. Design Example

The fluorescent lamp used in this investigation was a 40 W General Electric type F40D/2 with $P_{\text{lamp}} = 40$ W. $V_{\text{in}} = 24$ V, $I_{\text{lamp}_{(\text{rms})}} = 0.45$ A, $V_{\text{ig}_{\text{pk}}} = 160$ V, $I_{h_{(\text{rms})}} = 0.46$ A, $f_s = 300$ kHz, $n = 9$, $I^*_{\text{load}} = 2.4$, $R_{\text{lamp}} = 226.3\ \Omega$, $R^* = 0.2, (f_o/f_s) = 1.1$, $f_o = 330$ kHz, $L_r = 6.8\ \mu$H, $C_r = 34.2$ nF, $C_{\text{ig}} = 1.8$ nF, $f_{s_{\text{ig}}} = 361.5$ kHz, $I_{\text{Qm}} = 6.4$ A, $I_{\text{Dm}} = 4.4$ A, $V_{Q_m} = V_{D_m} = 81$ V, the transistors were type IRFP250, the diodes were type MUR140, $V_{Lr_{\max}} = 81$ V, $I_{Lr_{(\text{rms})}} = 4.2$ A, $V_{Tr_{\max}} = 15$ V, $I_{Tr_{(\text{rms})}} = 4.2$ A, $L_{\text{in}} = 27.2\ \mu$H, $V_{L\text{in}_{\max}} = 17$ V, $I_{L\text{in}_{(\text{rms})}} = 1.96$ A. The magnetic materiel of the inductors (L_r), (L_{in}) and transformer (T_2) was 3F3 (Philips). $V_{\text{Cr}_{\max}} = 81$ V. C_r and C_{ig} were Silver Mica capacitors.

D. Metal Halide Discharge (MHD) Lamps

Recently, there has been an increasing interest in MHD lamps which are highly efficient and have a desirable luminance spectrum [5]. MHD lamps belong to the class of high–pressure discharge lamps [9] in contrast to fluorescence lamps which are low pressure lamps [1]. The main difference in the electrical characteristics between the two group are related to the ignition voltage requirements (which are beyond the scope of this paper) and the susceptibility of the high-pressure discharge lamps to acoustic resonance [9]. The acoustic resonance is related to the dimension of the arc and the internal pressure [10]. As a result of the vulnerability of the lamp to internal pressure waves, the possibility of driving commercial MHD lamps is limited to some acoustic-resonant free frequency windows. It has been shown though, that at excitation frequencies above ca. 100 kHz, MHD lamps are free of the acoustic resonance problem [5]. This was verified in the present study by driving a commercial MHD lamp (Sylvania type H38AV-100/DX-100 W) by the proposed CS-PPRI that was operated at 300 kHz. It was found that at this frequency the operation is stable while the lamp characteristic is practically purely resistive (Fig. 10(b)).

VI. Conclusion

The results of the present study suggest that the CS-PPRI is a viable alternative for the realization of high-frequency current sources. The inherent ZVS characteristic of the proposed topology permits efficient operation at high frequency, possibly to 1 MHz, with commercially available electronic devices and magnetic materials. The proposed CS-PPRI is particularly useful as a driver for low and high- pressure discharge lamps which need to be fed by a current source. The advantage of this approach over previously described topologies is that it eliminates the need for an extra (inductive or capacitive) ballast. That is, there is no need to generate a much higher voltage and then to limit the current by a series impedance. In the proposed CS-PPRI the current is a function of the frequency ratio (f_o/f_s), a feature that can be used to realize a fluorescent lamp dimmer. The proposed model for the resistance of a fluorescent lamp can be useful in the design of electronic ballasts for these non linear devices.

The main limitation of the proposed CS-PPRI is the relatively high-voltage stress on the main switches. Since the maximum voltage is at least πV_{in} [7] practical considerations would therefore limit the input voltage to about 150 V when current MOSFET devices are used.

References

[1] W. Elenbaas, Ed., *Fluorescent Lamps* London: Macmillan, 1971.

[2] J. Spangler, B. Hussain, and A. K. Behera, "Electronic fluorescent ballast using a power factor correction techniques for loads greater than 300 watts," in *Proc. APEC-91*, Mar. 1991, pp. 393–399.

[3] E. E. Hammer, "High frequency characteristics of fluorescent lamp up to 500 kHz," *J. Illuminating Eng. Soc.*, pp. 52–61, Winter 1987.

[4] W. R. Alling, "Important design parameters for solid-state ballasts," *IEEE Trans. Ind. Applicat.*, vol. 25, no. 2, pp. 203–207, Mar./Apr. 1989.

[5] H-J. Faehnrich and E. Rasch, "Electronic ballasts for metal halide lamps," *J. Illuminating Eng. Soc.*, pp. 131–140, Summer 1988.

[6] D. V. Divan, "Design considerations for very high frequency resonant mode dc/dc converters," *IEEE Trans. Power Electron.*, vol. PE-2, no.1, pp. 45–54, Jan. 1987.

[7] G. Ivensky, A. Abramovitz, M. Gulko, and S. Ben-Yaakov, "A resonant dc-dc transformer," *IEEE Trans. Aerosp. Electron. Syst.* to be published.

[8] G. Ivensky, M. Gulko, and S. Ben-Yaakov, "Current-fed multi-resonant dc-dc converter," in *Proc. APEC-93* (San Diego, CA), Mar. 1993, pp. 58–64.

[9] J. F. Waymouth, *Electric Discharge Lamps*. Cambridge, MA: MIT Press, 1971.

[10] S. Wada, A. Okada, and S. Morii, "Study of HID lamps with reduced acoustic resonances," *J. Illuminating Eng. Soc.*, pp. 162–175, Winter 1987.

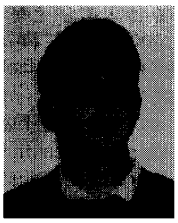

Michael Gulko was born in Moscow, USSR, in 1965. He received the B.Sc. degree in electrical engineering from the Communication Institute of Moscow, USSR, in 1988.

He is presently carrying out a research program in power electronics and circuit design as part of his M.Sc. degree studies at the Department of Electrical and Computer Engineering, Ben-Gurion University of the Negev, Beer-Sheva, Israel.

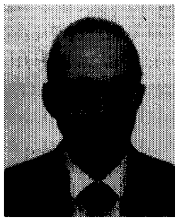

Shmuel (Sam) Ben-Yaakov (M'87) was born in Tel Aviv, Israel, in 1939. He received the B.Sc. degree in electrical engineering from the Technion, Haifa, Israel, in 1961, and the M.S. and Ph.D. degrees in engineering from the University of California, Los Angeles, in 1967 and 1970, respectively.

He is presently a Professor in the Department of Electrical and Computer Engineering, Ben-Gurion University of the Negev, Beer-Sheva, Israel, and served as the Chairman of that department during the period 1985–1989. His current research interests include switch mode converters, expert system for electronic design, microsensors, electronic instrumentation, signal processing, and engineering education.